applied sciences

MDPI

Article

Fe_3O_4-Water Nanofluid Free Convection within an Inclined 2D Rectangular Enclosure Heated by Solar Energy Using Finned Absorber Plate

Rached Nciri [1], Yahya Ali Rothan [2], Faouzi Nasri [3,4,*] and Chaouki Ali [4,5]

[1] Department of Mechanical Engineering, Higher Institute of Technological Studies of Gafsa, General Directorate of Technological Studies, Radès Médina 2098, Tunisia; rachednciri@yahoo.fr
[2] Mechanical Engineering Department, Faculty of Engineering, Jazan University, Jazan 82822, Saudi Arabia; yrothan@jazanu.edu.sa
[3] Mechanical Engineering Department, College of Engineering, University of Bisha, Bisha 61922, Saudi Arabia
[4] Laboratory of Electro-Mechanical Systems (LASEM), National Engineering School of Sfax-ENIS, B.P. W3038, University of Sfax, Sfax 3038, Tunisia; chaouki.ali.fsg@gmail.com
[5] Department of Technological Studies, Faculty of Sciences Gafsa, University of Gafsa, Gafsa 2112, Tunisia
* Correspondence: nasrifaouzi@yahoo.fr

Featured Application: The specific application of this work is particularly useful for promoting industrial applications working on solar energy storage and transfer. In fact, the investigated nanofluid enclosure presents a finned absorber plate heated by solar energy and considered as a hot top wall. The fins below the absorber plate permit to enhance the heat transfer from the hot absorber plate to the nanofluid. Cold temperatures are imposed partially on right and left walls, while the remaining walls are insulated. The effects of Rayleigh number, enclosure inclination and fins height on nanofluid flow and heat transfer are investigated.

Abstract: This work investigates a hydrodynamic problem involving the Fe_3O_4-Water nanofluid. The novelty of this investigation lies in the fact that the nanofluid free convection is evaluated within a specific rectangular enclosure having a finned absorber plate as the top wall, heated by solar energy. The fins below the absorber plate permit to enhance heat transfer towards the nanofluid. A numerical simulation is carried out in order to predict the influence of Rayleigh number, nanofluid layer position, enclosure inclination angle, and absorber plate fins height on the nanofluid flow (in terms of streamlines and velocity magnitude) and heat transfer (in terms of temperature and Nusselt number divided by a certain thermal conductivity ratio). Numerical results show a nanofluid buoyancy enhancement and a temperature distribution homogenization, when the Rayleigh number increases, all the more important and pushed to the right area of the enclosure, as the inclination angle of the enclosure is higher. For relatively low fin heights, the nanofluid buoyancy enhancement is all the more important and pushed to the right area of the enclosure as the inclination angle is high. As the fin height increases, the temperature distribution becomes more homogenous.

Keywords: natural convection; finned absorber plate; specific cavity; streamlines; Rayleigh number; Hartmann number

check for updates

Citation: Nciri, R.; Ali Rothan, Y.; Nasri, F.; Ali, C. Fe_3O_4-Water Nanofluid Free Convection within an Inclined 2D Rectangular Enclosure Heated by Solar Energy Using Finned Absorber Plate. *Appl. Sci.* **2021**, *11*, 486. https://doi.org/10.3390/app11020486

Received: 3 December 2020
Accepted: 30 December 2020
Published: 6 January 2021

Publisher's Note: MDPI stays neutral with regard to jurisdictional claims in published maps and institutional affiliations.

Copyright: © 2021 by the authors. Licensee MDPI, Basel, Switzerland. This article is an open access article distributed under the terms and conditions of the Creative Commons Attribution (CC BY) license (https://creativecommons.org/licenses/by/4.0/).

1. Introduction

Nanofluids [1–3] are used more and more in industrial heat transfer applications thanks to their thermo-physical properties, characterized by good capacity to store heat, without considerably increasing the temperature, and good thermal conductivity. This is ensured by the fact that a nanofluid consists of a base fluid, having good heat capacity [4], in which suspended nanoparticles, having very good thermal conductivity [5], are dissolved. In this way, nanofluids combine two major thermo-physical properties (high heat capacity and thermal conductivity) permitting an enhanced heat transfer.

The literature of the last three years on nanofluids free convection presents some interesting works. Figure 1 is presented in order to better understand the design description of each of these works (reference is added under each design description). Dwesh K. Singh [6] numerically investigated the free convection within a rectangular cavity filled with a Multi-Walled Carbon NanoTubes (MWCNT)-Water nanofluid. A temperature undulation is imposed at the left wall. The effects of cavity and nanoparticle aspect ratios on free convection are investigated. Results show that the minimum MWCNT diameter (maximum MWCNT aspect ratio) gives better heat transfer. An appropriate Rayleigh number range that gives better heat transfer is observed for various undulation temperatures at the left wall.

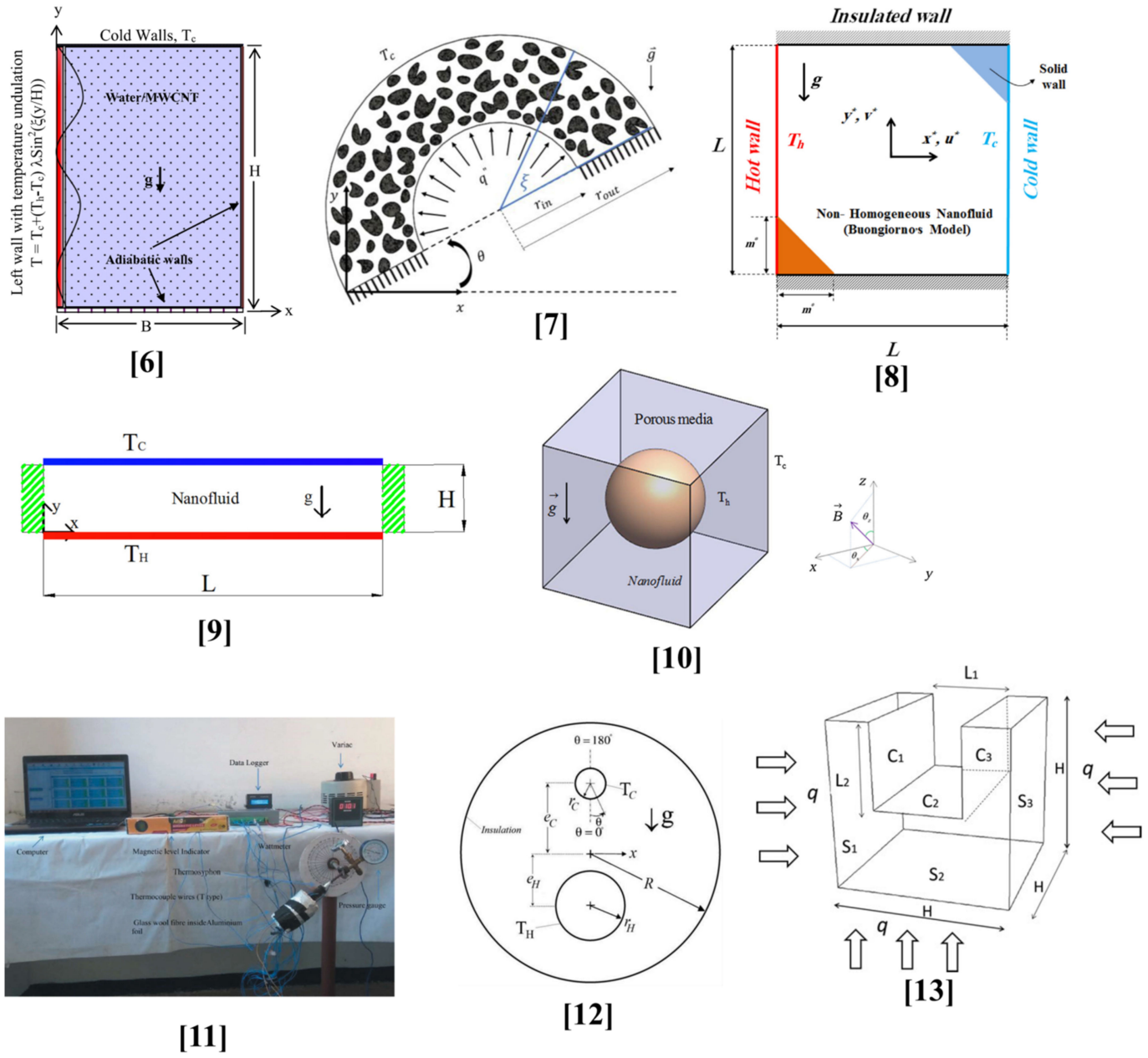


Figure 1. Design description of the works presented in the literature review.

Saber Yekani Motlagh et al. [7] applied Finite Volume Method and SIMPLE algorithm in order to numerically investigate two-phase free convection, within an inclined porous semi-annulus enclosure filled with Fe_3O_4-Water nanofluid. The effects of enclosure inclination angle, porous Rayleigh number and nanoparticles volume fraction on nanofluid flow

and heat transfer are investigated. Results show that the Nusselt number increases when nanoparticle volume fraction and porosity number increase, while the heat transfer rate decreases when the enclosure inclination angle increases at high porous Rayleigh numbers.

S.M. Hashem Zadeh et al. [8] numerically investigated the free convection (flow and heat transfer) within a cavity, with conjugate triangular blocks, filled with nanofluids. The effects of Rayleigh number, thermal conductivity ratio, thermal viscosity, Brownian motion, thermophoresis, and thickness and positions of the triangular blocks on nanofluid flow and heat transfer, are investigated. Results show that triangular blocks enhance the heat transfer rate when they are not placed in the reverse position. In addition, the average Nusselt number increases when the thermal conductivity ratio decreases.

Mohammad Reza Safaei et al. [9] implemented the Lattice Boltzman Method in order to numerically investigate the interaction between Al_2O_3-Water nanofluid thermal radiation and free convection in a 2D shallow cavity. The effects of emissivity and Rayleigh number on nanofluid flow and radiated/free convection heat transfer are investigated. Results show that the Nusselt number of the total radiation and free convection heat transfer increases when the Rayleigh number and the emissivity increase. Thus, the coupling between radiation and free convection affects the flow and enhances the Nusselt number.

M. Sheikholeslami et al. [10] implemented the Lattice Boltzman Method in order to numerically investigate the free convection within a 3D porous cavity with hot sphere obstacles, subjected to Lorenz forces and filled with Al_2O_3-Water nanofluid. The effects of Darcy number, Hartmann number, and Rayleigh number on the nanofluid heat transfer were evaluated. Results show that Lorenz forces enhance conduction at the expense of convection.

Sidhartha Das et al. [11] experimentally investigated the heat transfer enhancement within a thermosyphon exploiting TiO_2-Water nanofluid natural convection. The effects of heat input, inclination angle, and TiO_2 nanoparticles concentration on heat transfer (thermosyphon cooling) are studied and compared to the heat transfer carried out when using simple deionized water. Results show that the use of nanofluids reduces the wall temperature distribution and the thermosyphon thermal resistance. Thus, the performance of thermosyphon cooling is enhanced.

Ebrahim Khalili et al. [12] numerically investigated the natural convection within the Al_2O_3-Water nanofluid filled in a circular enclosure that contains two horizontal cylinders. The effects of nanoparticle loading percentage and Rayleigh number on heat transfer are investigated. Results show that the heat transfer is enhanced for high nanoparticles concentration. The average Nusselt number increases when Rayleigh number increases. Thus, the use of alumina nanofluid gives much better heat transfer than the use of pure water.

Lotfi Snoussi et al. [13] carried out a numerical comparison investigation about heat transfer by natural convection within a U-shaped enclosure, filled with Cu-Water and Al_2O_3-Water nanofluids. The effects of natural convection and geometric parameter on average Nusselt number are studied. The influence of Rayleigh number on the heat transfer within Al_2O_3-Water nanofluid is investigated. Results show that the heat transfer is improved when nanoparticle volume fraction and Rayleigh number increase and when the cooled wall length is extended.

This work aims to numerically investigate the flow and the heat transfer within a specific rectangular enclosure, filled with Fe_3O_4-Water nanofluid. The specificity of the enclosure lies in the fact that it has a finned absorber plate, as a top wall, heated by solar energy. The fins below the absorber plate permit to enhance the heat transfer towards the nanofluid. The effects of Rayleigh number, enclosure inclination angle and fins height on nanofluid flow and heat transfer are studied.

Section 2 of this article states and explains the problem in detail. The mathematical model that governs the hydrodynamic nanofluid problem as well as its dimensionless form is elaborated in Section 3. The numerical approach and validation are presented in Section 4. Section 5 presents numerical simulation results as well as their interpretation. Section 6 concludes the main findings of this work.

2. Problem Statement

Figure 2 depicts the investigated nanofluid hydrodynamic problem.

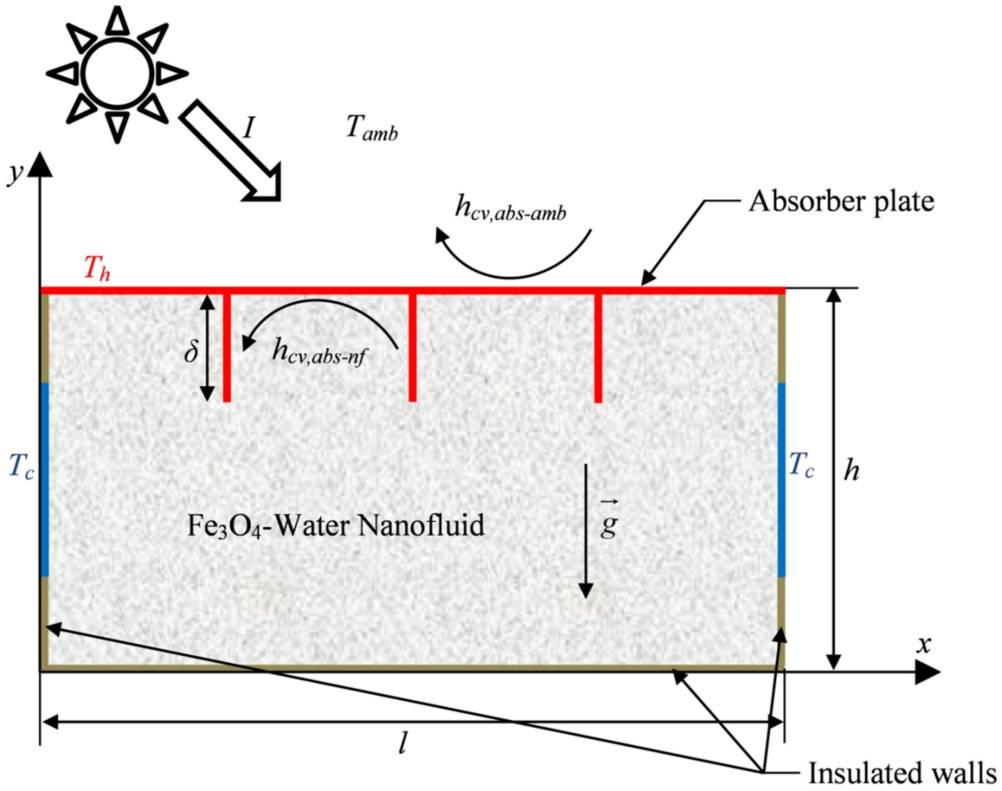


Figure 2. Schematic of the Fe_3O_4-Water nanofluid filled 2D rectangular enclosure heated by solar energy using finned absorber plate.

It is a rectangular enclosure, with a length l and a height h, filled with Fe_3O_4-Water nanofluid. The top wall of the enclosure is a finned absorber plate. This research work investigated various heights for the fins, such as $\delta = 0,\ h/8,\ h/4,\ h/2$. A fin height $\delta = 0$ means obviously that the considered absorber plate is without fins. The absorber, kept at a constant hot temperature T_h, is heated by solar energy (solar irradiance I), and it transfers heat by convection to the nanofluid. Fins permit to enhance the heat transfer from the heated absorber plate to the Fe_3O_4-Water nanofluid. Parts of right and left walls are maintained at a constant cold temperature T_c. The remaining wall parts of the enclosure are insulated.

The studied enclosure presents the specificity of having an imposed hot temperature coming from an absorber plate (top wall of the enclosure), heated at the top by solar energy. The inclination angle of the plate facing the sun's ray affects considerably the amount of solar energy kept by the absorber plate, and consequently the hot temperature imposed to the enclosure. Thus, it makes sense to consider several inclination angles for the enclosure in order to vary the imposed hot temperature. It is to note that the optimum inclination angle for a flat plate solar collector varies from 0° to 80° depending on the latitude of the location and the day number of the year [14]. The investigated nanofluid enclosure was, hence, inclined relative to the horizontal by several angles: $\gamma = 0°$, $\gamma = 15°$, $\gamma = 30°$ and $\gamma = 45°$. The investigated inclination angle ($[0°, 45°]$) was within this optimum inclination angle range ($[0°,80°]$), and it permitted to ensure a maximum solar energy collection during a typical day time in the region of Gafsa, Tunisia (34°25′52.1076″ N and 8°46′32.3616″ E).

The solid volume fraction of the investigated nanofluid is around $\phi = 0.05$. It is to note that we used a solid volume fraction not exceeding a threshold of 0.1 in order to avoid nanoparticles precipitation problems that may occur in nanofluids. The Prandtl

number of the Fe_3O_4–water nanofluid was the same as the one associated to its base fluid (water). Hence, the investigated Prandtl number was around Pr = 7. The Rayleigh number of the investigated nanofluid varied as Ra = 10^3, Ra = 10^4, and Ra = 10^5. These relatively low values of Rayleigh number allow the nanofluid to remain in a laminar flow. This avoids chaotic changes in pressure and flow velocity that characterize turbulent flows. Thus, the simulation numerical results will be more significant.

3. Mathematical Modeling

3.1. Physical Hydrodynamic Problem

The numerical investigation of nanofluid flow and heat transfer is governed by Navier–Stokes equations (momentum conservation) supported by the continuity equation (mass conservation) and the energy conservation equation [15–17]. Some assumptions are considered when elaborating the mathematical modeling of the investigated nanofluid hydrodynamic problem:

- The nanofluid is considered Newtonian, incompressible and in thermal equilibrium.
- The nanofluid flow is considered 2D, steady, and laminar.
- The Boussinesq approximation is adopted for the density variation in the buoyancy-driven flow.

Continuity equation

$$\frac{\partial u}{\partial x} + \frac{\partial v}{\partial y} = 0 \tag{1}$$

x-Momentum

$$\begin{aligned} \rho_{nf} u \tfrac{\partial u}{\partial x} + \rho_{nf} v \tfrac{\partial u}{\partial y} = \; & -\tfrac{\partial p}{\partial x} + \tfrac{\partial}{\partial x}\left(\mu_{nf} \tfrac{\partial u}{\partial x}\right) + \tfrac{\partial}{\partial y}\left(\mu_{nf} \tfrac{\partial u}{\partial y}\right) \\ & + (\rho\beta)_{nf} g (T - T_c) \sin(\gamma) \end{aligned} \tag{2}$$

y-Momentum

$$\begin{aligned} \rho_{nf} u \tfrac{\partial u}{\partial x} + \rho_{nf} v \tfrac{\partial u}{\partial y} = \; & -\tfrac{\partial p}{\partial x} + \tfrac{\partial}{\partial x}\left(\mu_{nf} \tfrac{\partial u}{\partial x}\right) + \tfrac{\partial}{\partial y}\left(\mu_{nf} \tfrac{\partial u}{\partial y}\right) \\ & + (\rho\beta)_{nf} g (T - T_c) \cos(\gamma) \end{aligned} \tag{3}$$

Energy conservation equation

$$u \frac{\partial T}{\partial x} + v \frac{\partial T}{\partial y} = \alpha_{nf} \left(\frac{\partial^2 T}{\partial x^2} + \frac{\partial^2 T}{\partial y^2} \right) \tag{4}$$

The effective nanofluid mechanical properties are determined based on the mechanical properties of base fluid and nanoparticles as follows:

$$\rho_{nf} = (1 - \phi)\rho_f + \phi\rho_p \tag{5}$$

$$(\rho C_p)_{nf} = (1 - \phi)(\rho C_p)_f + \phi(\rho C_p)_p \tag{6}$$

$$(\rho\beta)_{nf} = (1 - \phi)(\rho\beta)_f + \phi(\rho\beta)_p \tag{7}$$

$$\alpha_{nf} = \frac{k_{nf}}{(\rho C_p)_{nf}} \tag{8}$$

$$\mu_{nf} = \frac{\mu_f}{(1 - \phi)^{\frac{5}{2}}} \tag{9}$$

$$k_{nf} = k_f \frac{k_p + 2k_f + 2\phi\left(k_p - k_f\right)}{k_p + 2k_f + \phi\left(k_f - k_p\right)} \tag{10}$$

Boundary conditions

The boundary conditions, applied on the investigated nanofluid, are set as follows:

- On the top wall (absorber plate):

$$\left| \begin{array}{c} u(x,h) = v(x,h) = 0 \\ T(x,h) = T_h \end{array} \right.$$

- On the bottom wall:

$$\left| \begin{array}{c} u(x,0) = v(x,0) = 0 \\ \frac{\partial T}{\partial y}\Big|_{y=0} = 0 \end{array} \right.$$

- On the left wall:

$$\left| \begin{array}{c} u(0,y) = v(0,y) = 0 \\ T(0,y) = T_c; \frac{h}{4} \le y \le \frac{3h}{4} \\ \frac{\partial T}{\partial x}\Big|_{x=0} = 0; y < \frac{h}{4} \text{ and } y > \frac{3h}{4} \end{array} \right.$$

- On the right wall:

$$\left| \begin{array}{c} u(l,y) = v(l,y) = 0 \\ T(l,y) = T_c; \frac{h}{4} \le y \le \frac{3h}{4} \\ \frac{\partial T}{\partial x}\Big|_{x=l} = 0; y < \frac{h}{4} \text{ and } y > \frac{3h}{4} \end{array} \right.$$

3.2. Dimensionless Nanofluid Hydrodynamic Problem

It is more convenient to handle the dimensionless form of nanofluid hydrodynamic problems [18–20]. In order to adimensionalize the investigated problem, the following dimensionless variables are used:

$$X = \frac{x}{l} \tag{11}$$

$$Y = \frac{y}{l} \tag{12}$$

$$U = \frac{ul}{\alpha_{nf}} \tag{13}$$

$$V = \frac{vl}{\alpha_{nf}} \tag{14}$$

$$P = \frac{pl^2}{\rho_{nf}\alpha_{nf}^2} \tag{15}$$

$$\alpha_{nf} = \frac{k_{nf}}{\rho_{nf}C_{nf}} \tag{16}$$

$$\theta = \frac{T - T_c}{T_h - T_c} \tag{17}$$

The resulting dimensionless equations, that govern the nanofluid hydrodynamic problem, are written as:

$$\frac{\partial U}{\partial X} + \frac{\partial V}{\partial Y} = 0 \tag{18}$$

$$U\frac{\partial U}{\partial X} + V\frac{\partial U}{\partial Y} = -\frac{\partial P}{\partial X} + \mathrm{Pr}\left(\frac{\partial^2 U}{\partial X^2} + \frac{\partial^2 U}{\partial Y^2}\right) + \mathrm{RaPr}\theta\sin(\gamma) \tag{19}$$

$$U\frac{\partial V}{\partial X} + V\frac{\partial V}{\partial Y} = -\frac{\partial P}{\partial Y} + \mathrm{Pr}\left(\frac{\partial^2 V}{\partial X^2} + \frac{\partial^2 V}{\partial Y^2}\right) + \mathrm{RaPr}\theta\cos(\gamma) \tag{20}$$

$$U\frac{\partial\theta}{\partial X}+V\frac{\partial\theta}{\partial Y}=\left(\frac{\partial^2\theta}{\partial X^2}+\frac{\partial^2\theta}{\partial Y^2}\right) \tag{21}$$

$$\mathrm{Ra}=\frac{g\beta_{nf}(T_h-T_c)l^3}{\nu_{nf}\alpha_{nf}} \tag{22}$$

$$\mathrm{Pr}=\frac{\nu_{nf}}{\alpha_{nf}}=\frac{\mu_{nf}}{\rho_{nf}\alpha_{nf}} \tag{23}$$

4. Numerical Approach and Validation

The finite element method was numerically implemented in order to solve the partial differential equations governing the nanofluid flow and heat transfer (Navier–Stokes equations). The investigated nanofluid domain is discretized into a free triangular node mesh calibrated as predefined finer with a maximum and minimum element size around 0.014 and 2×10^{-4}, respectively. Three meshes, having a number of elements around 2422, 4036, and 10,584, were tested. The obtained numerical results for the investigated coarse and fine meshes were very close (the difference was less than 1%). The used complete mesh consisted of 10,584 elements. The relative tolerance was set small enough (around 10^{-5}) to guarantee the convergence. Figure 3 depicts the meshing used for the investigated nanofluid domain.

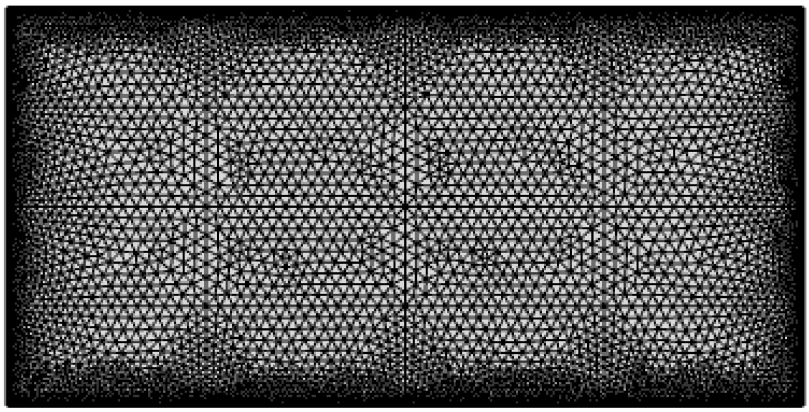


Figure 3. Free triangular node mesh applied to the investigated nanofluid domain.

The validation of the computer code was carried out by implementing the same problem investigated by Qi-Hong Deng and Juan-Juan Chang [21]. As it is depicted in Figure 4, a very good agreement was obtained between our numerical results and those presented in [21].

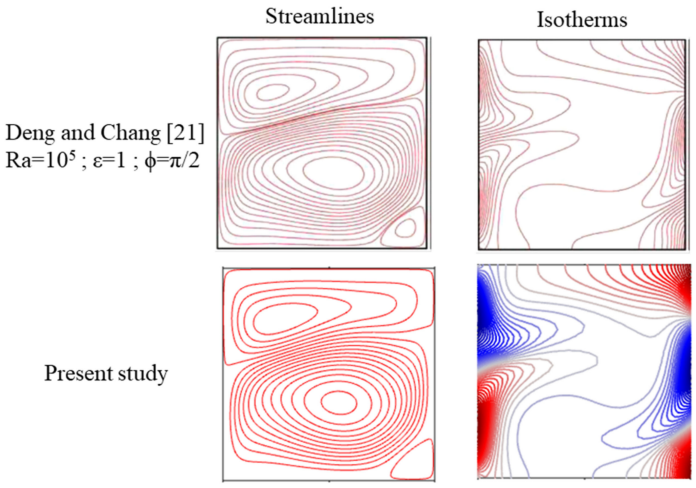


Figure 4. Results validation.

5. Numerical Simulation

Figures 5–7 depict the nanofluid velocity evolutions at several enclosure levels ($X = 0.25$, $X = 0.5$, $Y = 0.25$ and $Y = 0.5$) and for different Rayleigh numbers ($Ra = 10^3$, $Ra = 10^4$ and $Ra = 10^5$) and inclination angles (0°, 15°, 30° and 45°). When the inclination angle was 0°, the velocity evolutions were quite symmetric along the y-axis. The symmetry of the velocity evolution along the y-axis was more pronounced than the one along the x-axis. This gradually deteriorated going towards the highest inclination angles. For a relatively low Rayleigh number $Ra = 10^3$, and as the inclination angle increased, the higher extremum velocity globally decreased while the lower extremum globally increases at the level $X = 0.25$ and conversely at the level $X = 0.5$, along the y-axis. Along the x-axis, the higher and the lower extrema of velocity evolutions, for the different inclination angles, alternated around $X = 0.4$ at the level $Y = 0.25$ and globally triple alternated around $X = 0.2$ and $X = 0.75$ at the level $Y = 0.5$.

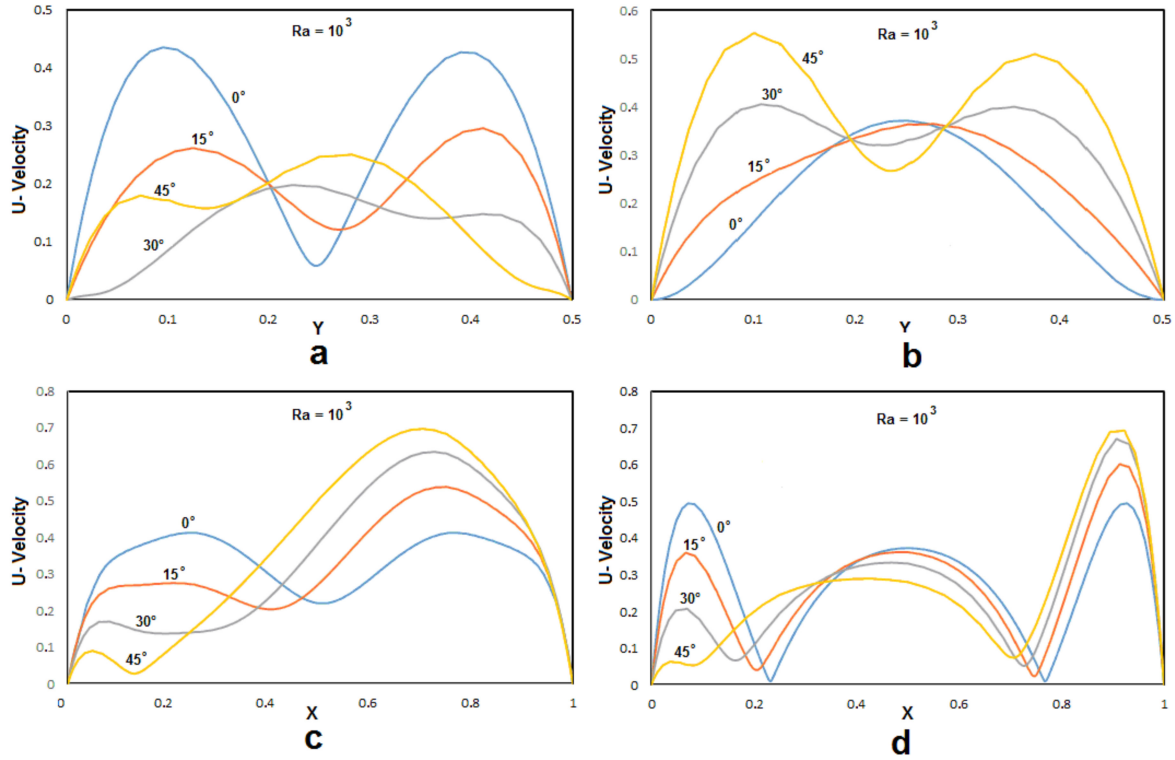


Figure 5. Nanofluid velocity evolutions at the levels: $X = 0.25$ (**a**) $X = 0.5$ (**b**) $Y = 0.25$ (**c**) $Y = 0.5$ (**d**) for a Rayleigh number $Ra = 10^3$.

As the Rayleigh number increased to a relatively moderate value $Ra = 10^4$, the evolutions of velocity along all the investigated directions (x-axis and y-axis) and at all the investigated levels ($X = 0.25$, $X = 0.5$, $Y = 0.25$, $Y = 0.5$) kept the same tendency as for the case when the Rayleigh number was relatively low. It is to note here that the higher and the lower extrema are drastically amplified.

For a relatively high Rayleigh number $Ra = 10^5$, and as the inclination angle increased, the higher and lower velocity extrema globally increased along the y-axis at the levels $X = 0.25$ and $X = 0.5$. Along the x-axis, and for the different inclination angles, the higher and lower velocity extrema alternated around $X = 0.35$ at the level $Y = 0.25$ and globally triple alternated around $X = 0.15$ and $X = 0.7$ at the level $Y = 0.5$.

Figure 8 depicts the heat transfer behavior of the nanofluid in terms of temperature and Nusselt number related to a certain thermal conductivity ratio κ. This κ ratio is defined by:

$$\kappa = -k_f / k_{nf} \tag{24}$$

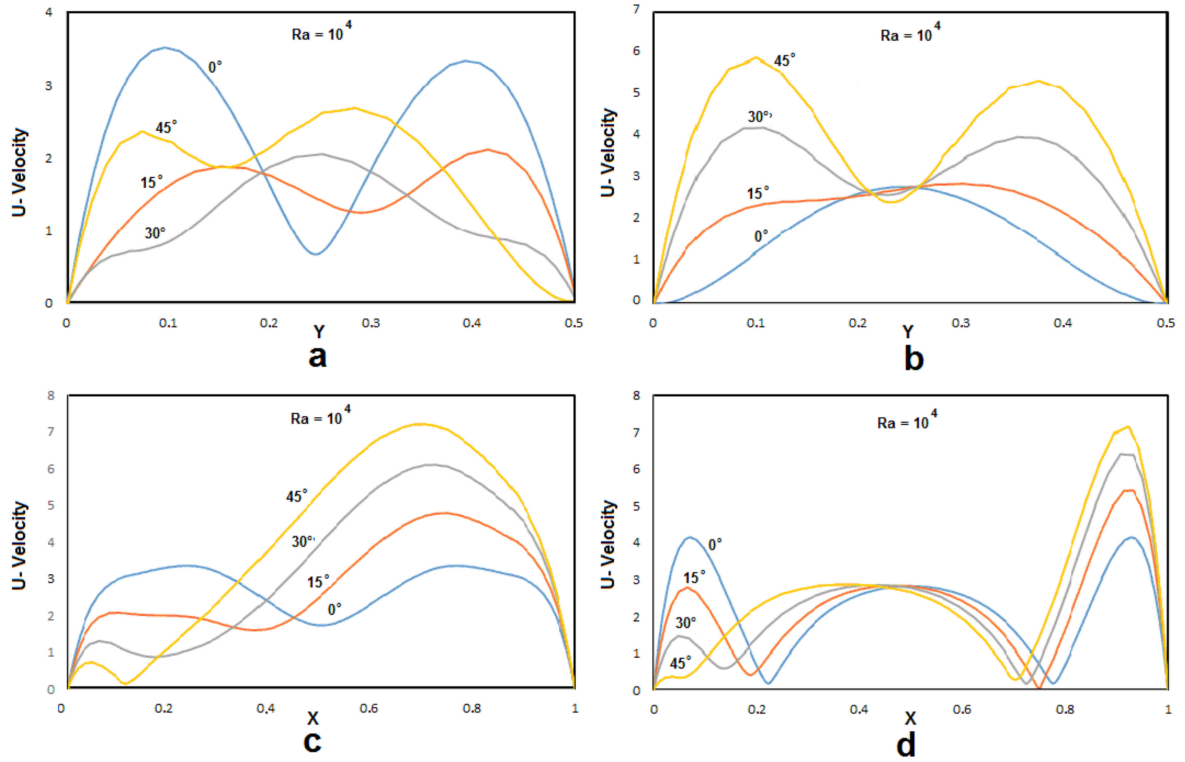


Figure 6. Nanofluid velocity evolutions at the levels: $X = 0.25$ (**a**) $X = 0.5$ (**b**) $Y = 0.25$ (**c**) $Y = 0.5$ (**d**) for a Rayleigh number $Ra = 10^4$.

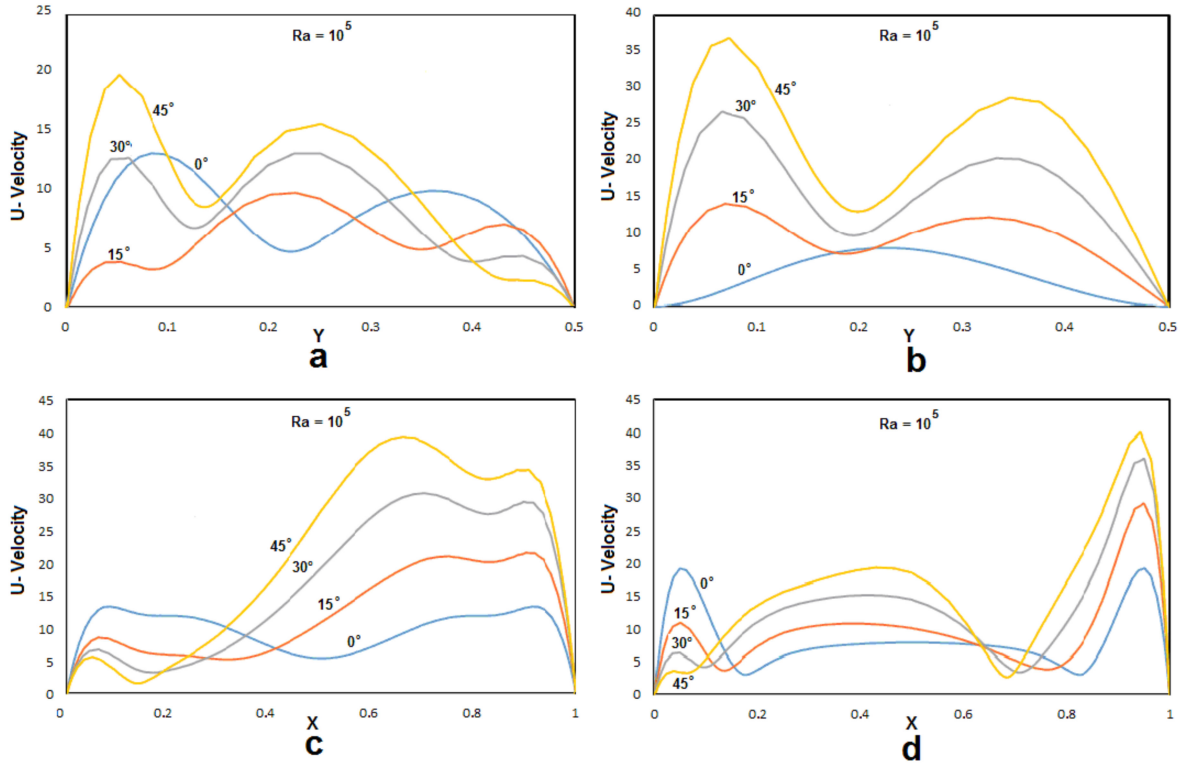


Figure 7. Nanofluid velocity evolutions at the levels: $X = 0.25$ (**a**) $X = 0.5$ (**b**) $Y = 0.25$ (**c**) $Y = 0.5$ (**d**) for a Rayleigh number $Ra = 10^5$.

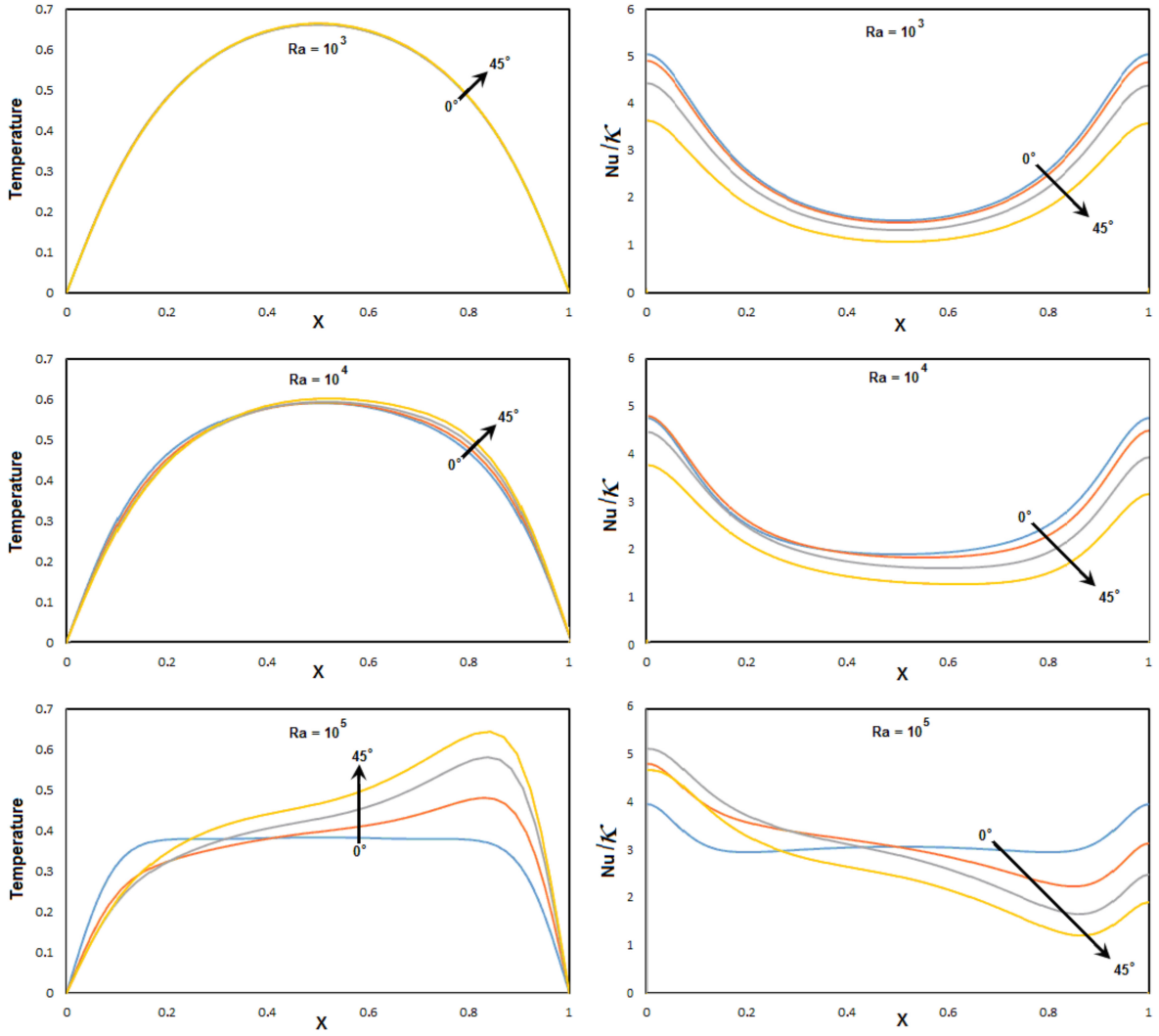


Figure 8. Nanofluid temperature and Nu/κ evolutions at the levels: $Y = 0.5$ (**right**) and $Y = 1$ (**left**) respectively.

The nanofluid temperature evolutions are depicted along the x-axis at the level $Y = 0.5$, for different Rayleigh numbers (Ra = 10^3, Ra = 10^4 and Ra = 10^5) and inclination angles (0°, 15°, 30°, and 45°). This temperature evolution depended on the inclination angle only for relatively higher Rayleigh number (in the order of Ra = 10^5). The nanofluid temperature globally increased as the inclination angle increases. The evolutions of the nanofluid Nusselt number Nu related to the thermal conductivity ratio κ are depicted along the x-axis at the level $Y = 1$, for different inclination angles (0°, 15°, 30° and 45°). This evolution globally decreased as the inclination angle increased. It is to note that the symmetry of the heat transfer behavior of the nanofluid along the x-axis gradually deteriorated going towards the highest inclination angles.

Figure 9 shows the combined effect of Rayleigh number and enclosure inclination angle on nanofluid streamlines, when there are no fins below the absorber plate ($\delta = 0$). The nanofluid streamlines presents two elliptical core vortices globally symmetric for an inclination angle $\gamma = 0°$. As the Rayleigh number increased from Ra = 10^3 to Ra = 10^5, the nanofluid buoyancy increased. As the enclosure inclination angle increases, the maximum buoyancy was pushed towards the right area of the enclosure (nanofluid streamlines gradually loses its symmetry), while the nanofluid flow in the left area of the enclosure became more laminar.

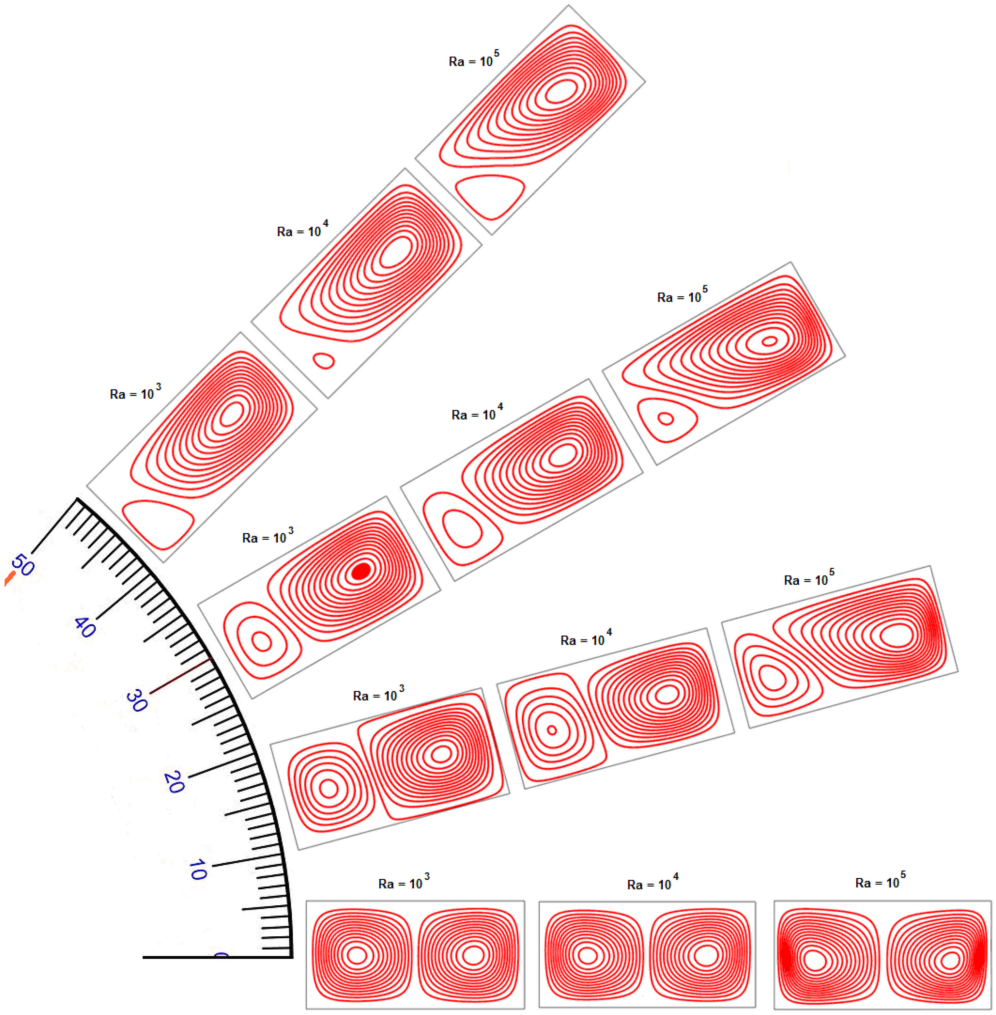


Figure 9. Effects of Rayleigh number and enclosure inclination angle on nanofluid streamlines.

Figure 10 shows the combined effect of Rayleigh number and enclosure inclination angle on nanofluid velocity magnitude distribution, when there are no fins below the absorber plate ($\delta = 0$). As the Rayleigh number increased from Ra = 10^3 to Ra = 10^5, the nanofluid velocity magnitude distribution became more homogenous, and its maximum value drastically increased from 0.5 to 19, 0.6 to 30, 0.7 to 36, and 0.8 to 45 for an inclination angle of $\gamma = 0°$, $\gamma = 15°$, $\gamma = 30°$ and $\gamma = 45°$, respectively. It is to note that the maximum nanofluid velocity magnitude was pushed towards the right area of the enclosure (nanofluid magnitude distribution gradually loses its symmetry) as the inclination angle increased.

Figure 11 shows the combined effect of Rayleigh number and enclosure inclination angle on nanofluid isotherms, when there are no fins below the absorber plate ($\delta = 0$). As the Rayleigh number increased from Ra = 10^3 to Ra = 10^5, the nanofluid temperature distribution became globally more homogenous, especially in the central area of the enclosure, away from walls where the cold and hot temperatures were imposed. It is to note that the most homogenous nanofluid temperature was pushed towards the right area of the enclosure as the inclination angle increased.

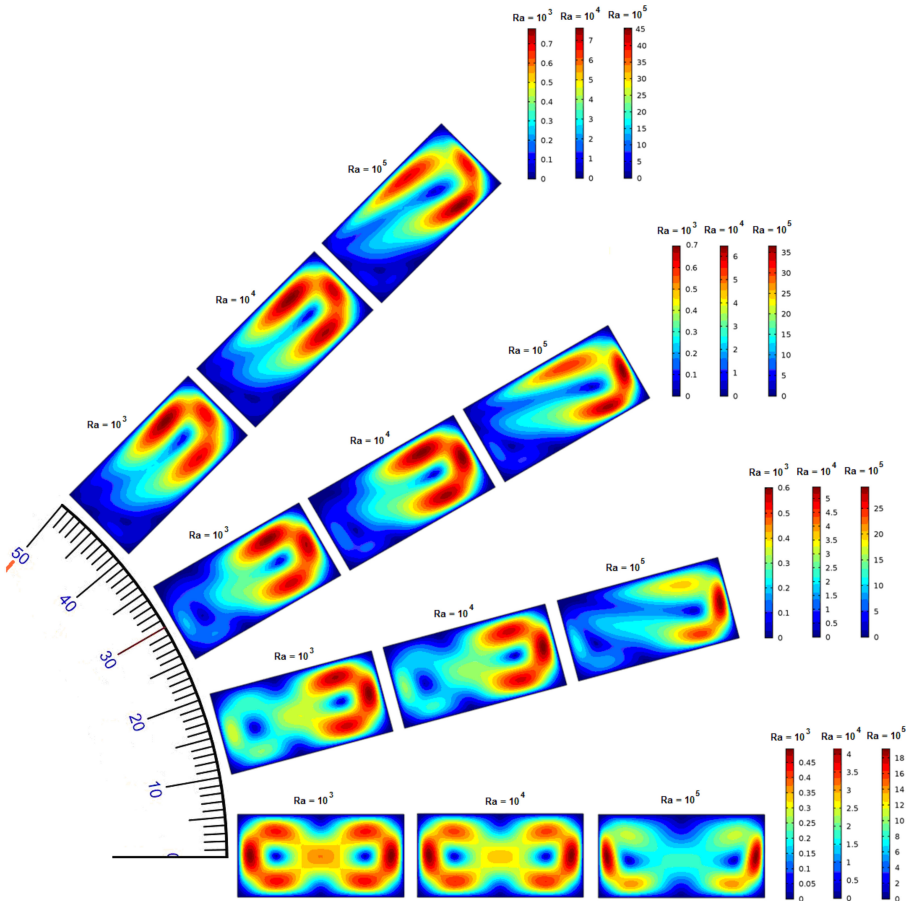


Figure 10. Effects of Rayleigh number and enclosure inclination angle on nanofluid velocity magnitude.

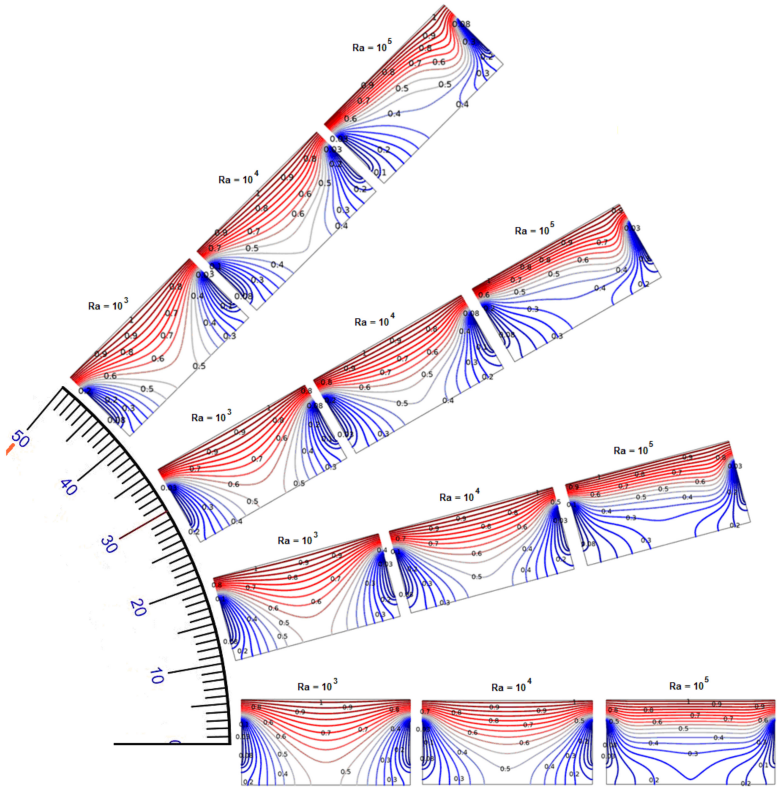


Figure 11. Effects of Rayleigh number and enclosure inclination angle on nanofluid isotherms.

Figure 12 shows the combined effect of fins height and enclosure inclination angle on nanofluid streamlines for a Rayleigh number Ra = 10^5. The nanofluid streamlines present two elliptical core vortices globally symmetric for an inclination angle $\gamma = 0°$, whatever the fins' height. As the inclination angle increased, buoyancy was pushed towards the right area of the enclosure (nanofluid streamlines gradually lose their symmetry), while the nanofluid flow in the left area of the enclosure became more laminar. This phenomenon was more pronounced for relatively low fin height. As the fin height increased from $\delta = \frac{h}{8}$ to $\delta = \frac{h}{2}$, the nanofluid buoyancy increased.

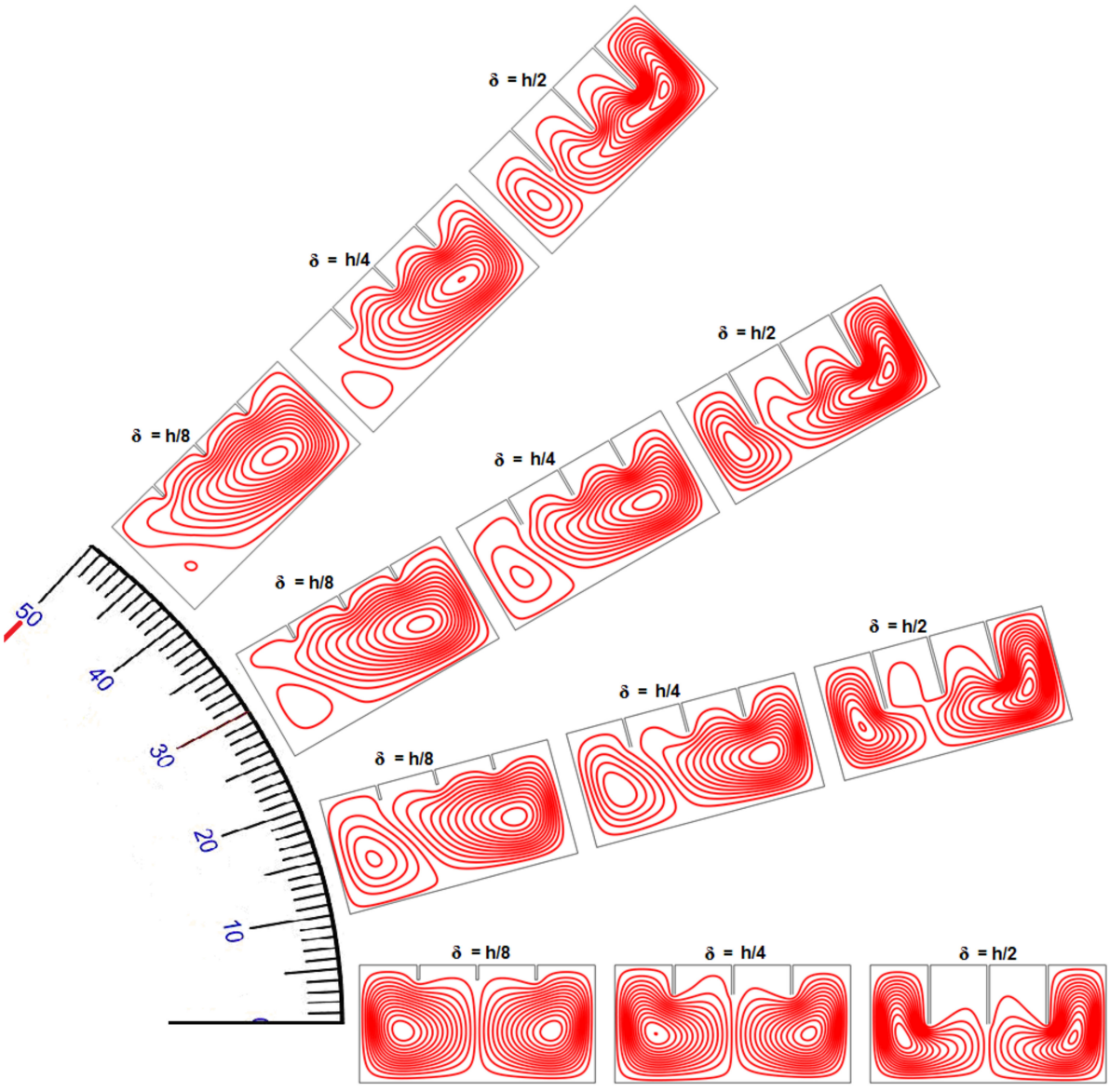


Figure 12. Effects of fin height and enclosure inclination angle on nanofluid streamlines.

Figure 13 shows the combined effect of fin height and enclosure inclination angle on nanofluid isotherms for a Rayleigh number Ra = 10^5. As the fin height increased from $\delta = \frac{h}{8}$ to $\delta = \frac{h}{2}$, the nanofluid temperature distribution became globally more homogenous, especially in the central area of the enclosure, away from walls where the cold and hot temperatures were imposed. It is to note that the most homogenous nanofluid temperature was pushed towards the right area of the enclosure as the inclination angle increased.

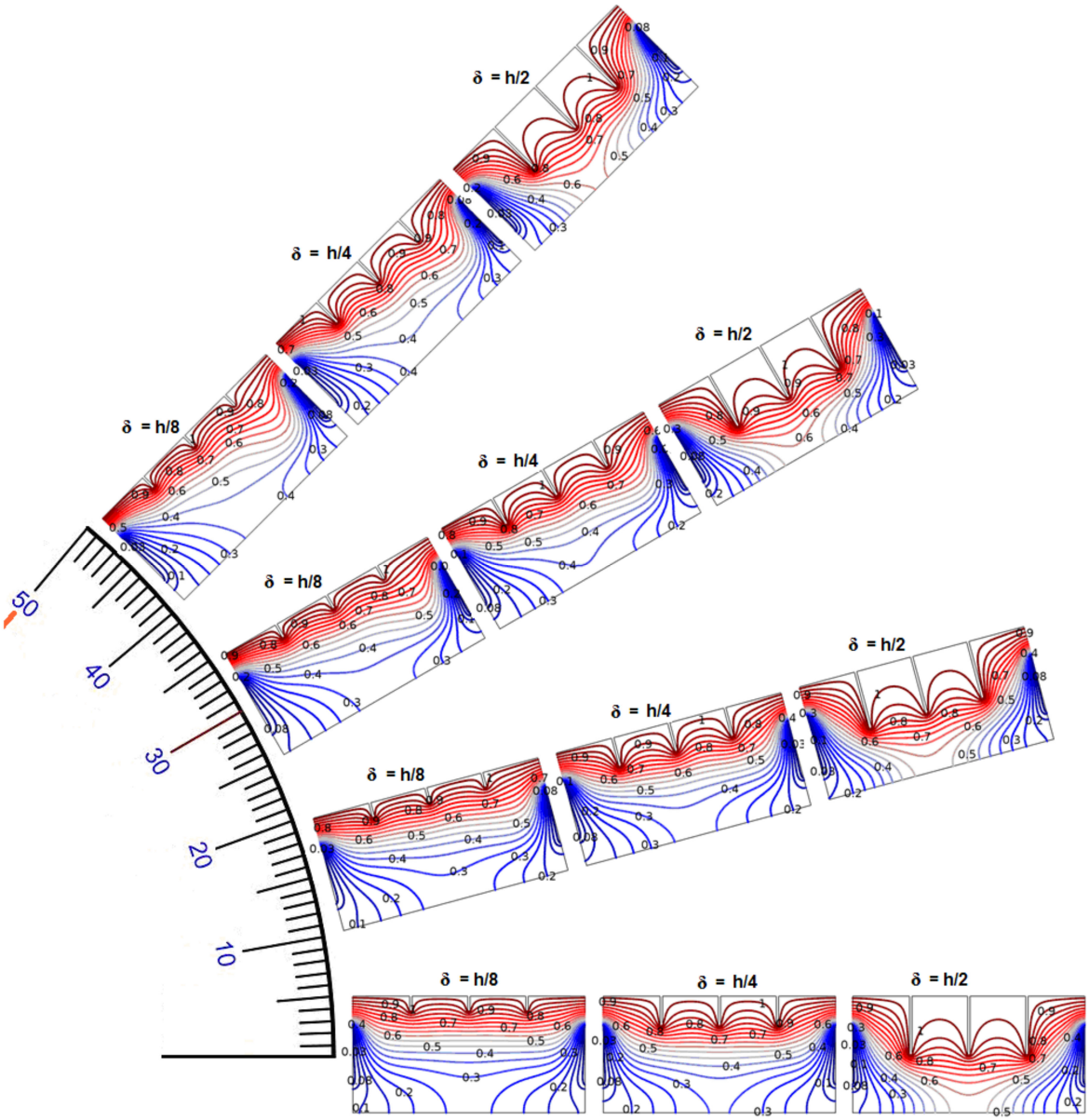


Figure 13. Effects of fins height and enclosure inclination angle on nanofluid isotherms.

6. Conclusions

The flow and heat transfer of the Fe_3O_4 nanofluid were investigated within a specific rectangular enclosure. The interest of the proposed study lies in the fact that the enclosure presents a finned absorber plate heated by solar energy and considered as a hot top wall. The fins below the absorber plate permit to enhance the heat transfer from the hot absorber plate to the nanofluid. Cold temperatures were imposed partially on right and left walls, while the remaining walls were insulated. The effects of Rayleigh number, enclosure inclination and fin height on nanofluid flow and heat transfer were investigated. Numerical simulations show that the symmetry of nanofluid velocity evolution along the y-axis was more noticeable than the one along the x-axis, and it progressively weakened going towards the highest enclosure inclination angles. As the Rayleigh number increased from Ra = 10^3 to Ra = 10^4, the higher and the lower extrema of nanofluid velocity evolutions were considerably amplified, keeping the same trend evolution. For a Rayleigh number Ra = 10^5, the higher and the lower extrema of nanofluid velocity evolutions globally increased along the y-axis and alternated along the x-axis. As the enclosure inclination

angles increased, the symmetry of nanofluid temperature and Nu/κ evolutions along the x-axis gradually deteriorate. Moreover, the nanofluid temperature globally increased, while the nanofluid Nu/κ globally decreased. It is to note that only for a relatively important Rayleigh number (in the order of Ra = 10^5), the nanofluid temperature varied (increased) as the enclosure inclination angle increased.

The numerical simulation of the combined effect of Rayleigh number and enclosure inclination angle showed that the nanofluid buoyancy and the velocity magnitude were considerably enhanced as the Rayleigh number increased from Ra = 10^3 to Ra = 10^5. The enhancement of velocity magnitude was all the more important as the enclosure inclination angle was higher. As the enclosure inclination angle increased from $\gamma = 0^\circ$ to $\gamma = 45^\circ$, the maximum nanofluid buoyancy and the maximum velocity magnitude were pushed towards the right area of the enclosure, while the nanofluid flow in the left area of the enclosure became more laminar. As the Rayleigh number increased from Ra = 10^3 to Ra = 10^5, the nanofluid temperature distribution became globally more homogenous, particularly in the central area of the enclosure. As the enclosure inclination angle increased from $\gamma = 0^\circ$ to $\gamma = 45^\circ$, the most homogenous nanofluid temperature was pushed towards the right area of the enclosure. The numerical simulation of the combined effect of fin height and enclosure inclination angle showed that the pushing of nanofluid buoyancy towards the right area of the enclosure, as the inclination angle increased, was more noticeable for relatively low fin heights. As the fin height increased from $\delta = \frac{h}{8}$ to $\delta = \frac{h}{2}$, the nanofluid temperature distribution became globally more homogenous, especially in the central area of the enclosure.

Author Contributions: Conceptualization, C.A.; methodology, R.N. and C.A., Y.A.R.; software, C.A.; completed literature review, R.N., Y.A.R. and F.N.; formal analysis, F.N., R.N. and Y.A.R.; investigation, F.N., Y.A.R. and R.N.; writing—original draft preparation, R.N., Y.A.R., F.N. and C.A.; writing—review and editing, R.N., Y.A.R. and F.N.; supervision, C.A. All authors have read and agreed to the published version of the manuscript.

Funding: This research was funded by Jazan University, Kingdom of Saudi Arabia.

Institutional Review Board Statement: Not applicable.

Informed Consent Statement: Not applicable.

Acknowledgments: We are grateful to Jazan University, Kingdom of Saudi Arabia for its financial support.

Conflicts of Interest: We declare, as authors of this article, that there is no conflict of interest.

Abbreviations

C_p	Specific heat capacity
g	Gravitational acceleration
k	Thermal conductivity
L	Characteristic length
p	Pressure
Pr	Prandtl number
Ra	Rayleigh number
T	Temperature
u	x-component of velocity
v	y-component of velocity
x	x-direction
y	y-direction
Greek symbols	
α	Thermal diffusivity
β	Coefficient of thermal expansion
δ	Height of the fin
ϕ	Solid volume fraction
γ	Inclination angle of the enclosure with respect to the horizontal
μ	Dynamic viscosity
θ	Dimensionless temperature
ρ	Density
ρC_p	Heat capacitance

$\rho\beta$	Thermal expansion
v	Kinematic viscosity
κ	$\kappa = -k_f/k_{nf}$ Thermal conductivity ratio
Subscripts	
c	Cold
f	Fluid
h	Hot
nf	Nanofluid
p	Particle
Capital letter	Dimensionless variable

References

1. Stephen, U.; Choi, S. Nanofluids: A New Field of Scientific Research and Innovative Applications. *Heat Transf. Eng.* **2008**, *29*, 429–431. [CrossRef]
2. Das, S.K.; Choi, S.U.S.; Patel, H.E. Heat Transfer in Nanofluids—A Review. *Heat Transf. Eng.* **2006**, *27*, 3–19. [CrossRef]
3. Hatami, M.; Jing, D. Chapter 1-Introduction to Nanofluids. In *Nanofluids, Mathematical, Numerical, and Experimental Analysis*; Academic Press: Cambridge, MA, USA, 2020; pp. 1–50. [CrossRef]
4. Sekhar, Y.R.; Sharma, K.V. Study of Viscosity and Specific Heat Capacity Characteristics of Water-Based Al_2O_3 Nanofluids at low Particle Concentrations. *J. Exp. Nanosci.* **2015**, *10*, 86–102. [CrossRef]
5. Yu, H.; France, D.V.; Routbort, J.L.; Choi, S.U.S. Review and Comparison of Nanofluid Thermal Conductivity and Heat Transfer Enhancements. *Heat Transf. Eng.* **2008**, *29*, 432–460. [CrossRef]
6. Singh, D.K. Free Convection with MWCNT/Water Nanofluid Having Varying Aspect Ratio of MWCNT Nanoparticle in Thermally Undulated. *Int. J. Mech. Sci.* **2020**, *178*, 105626. [CrossRef]
7. Motlagh, S.Y.; Golab, E.; Sadr, A.N. Two-Phase Modeling of the Free Convection of Nanofluid Inside the Inclined Porous Semi-Annulus Enclosure. *Int. J. Mech. Sci.* **2019**, *164*, 105183. [CrossRef]
8. Zadeh, S.M.H.; Sabour, M.; Sazgara, S.; Ghalambaz, M. Free Convection Flow and Heat Transfer of Nanofluids in A Cavity with Conjugate Solid Triangular Blocks: Employing Buongiorno's Mathematical Model. *Phys. A Stat. Mech. Appl.* **2020**, *583*, 122826. [CrossRef]
9. Safaei, M.R.; Karimipour, A.; Abdollahi, A.; Nguyen, T.K. The Investigation of Thermal Radiation and Free Convection Heat Transfer Mechanisms of Nanofluid Inside a Shallow Cavity by Lattice Boltzmann Method. *Phys. A Stat. Mech. Appl.* **2018**, *509*, 515–535. [CrossRef]
10. Sheikholeslami, M.; Shehzad, S.A.; Li, Z. Water Based Nanofluid Free Convection Heat Transfer in a Three Dimensional Porous Cavity with Hot Sphere Obstacle in Existence of Lorenz Forces. *Int. J. Heat Mass Transf.* **2018**, *125*, 375–386. [CrossRef]
11. Das, S.; Giri, A.; Samanta, S. Heat Transfer Enhancement in a Thermosyphon Using TiO2 Nanofluid through Natural Convection. *Energy Sources Part A Recov. Util. Environ. Eff.* **2020**, 1–18. [CrossRef]
12. Khalili, E.; Saboonchi, A.; Saghafian, M. Natural Convection of Al2O3 Nanofluid Between Two Horizontal Cylinders Inside a Circular Enclosure. *Heat Transf. Eng.* **2017**, *38*, 177–189. [CrossRef]
13. Snoussi, L.; Ouerfelli, N.; Chesneau, X.; Chamkha, A.J.; Belgacem, F.B.M.; Guizani, A. Natural Convection Heat Transfer in a Nanofluid Filled U-Shaped Enclosures: Numerical Investigations. *Heat Transf. Eng.* **2018**, *39*, 1450–1460. [CrossRef]
14. Stanciu, C.; Stanciu, D. Optimum Tilt Angle for Flat Plate Collectors All Over the World–A Declination Dependence Formula and Comparisons of Three Solar Radiation Models. *Energy Convers. Manag.* **2014**, *81*, 133–143. [CrossRef]
15. Nasri, F.; Rothan, Y.A.; Nciri, R.; Ali, C. MHD Natural Convection of A Fe3O4–Water Nanofluid within An Inside Round Diagonal Corner Square Cavity with Existence of Magnetic Source. *Appl. Sci.* **2020**, *10*, 3236. [CrossRef]
16. Girault, V.; Raviart, P.-A. Finite Element Approximation of the Navier-Stokes Equations. In *Lecture Notes in Mathematics*; Springer: Berlin, Germany, 1979; p. 208. ISBN 978-3-540-34856-6.
17. Sidik, N.A.C.; Yazid, M.N.A.W.M.; Samion, S.; Musa, M.N.; Mamat, R. Latest Development on Computational Approaches for nanofluid Flow Modeling: Navier–Stokes based multiphase models. *Int. Commun. Heat Mass Transf.* **2016**, *74*, 114–124. [CrossRef]
18. Kamyar, A.; Saidur, R.; Hasanuzzaman, M. Application of Computational Fluid Dynamics (CFD) for nanofluids. *Int. J. Heat Mass Transf.* **2012**, *55*, 4104–4115. [CrossRef]
19. Versteeg, H.; Malalasekra, W. *An Introduction to Computational Fluid Dynamics: The Finite Volume Method*, 2nd ed.; Prentice Hall: New York, NY, USA, 2007; ISBN 139780131274983.
20. Patankar, S.V. *Numerical Heat Transfer and Fluid Flow*, 1st ed.; CRC Press: Boca Raton, FL, USA, 1979; ISBN 9780891165224.
21. Deng, Q.-H.; Chang, J.-J. Natural Convection in A Rectangular Enclosure with Sinusoidal Temperature Distributions on Both Side Walls. *Numer. Heat Transf. Part A Appl.* **2008**, *54*, 507–524. [CrossRef]